Epoxymicheliolide, a novelguaiane-type sesquiterpene lactone, inhibits NF-κB/COX-2 signaling pathways by targeting leucine 281 and leucine 25 in IKKβ in renal cell carcinoma

JIABIN ZHU[1,2], JUN ZHAO[3], ZHENLONG YU[4], SANDEEP SHRESTHA[1], JING SONG[5], WENWEN LIU[5], WEN LAN[5], JINSHAN XING[6], SHUANG LIU[7], CHEN CHEN[8], MOMO CAO[9], XIUZHEN SUN[10], QI WANG[5] and XISHUANG SONG[1]

[1]Department of Urology, The First Affiliated Hospital, Dalian Medical University, Dalian, Liaoning 116011; [2]The Affiliated Renhe Hospital, China Three Gorges University, Yichang, Hubei 443000; [3]Department of Neurosurgery, The First Affiliated Hospital, Dalian Medical University, Dalian, Liaoning 116011; [4]College of Pharmacy, Dalian Medical University, Dalian, Liaoning 116044; Departments of [5]Respiratory Medicine, [6]Neurosurgery and [7]Gastroenterology, The Second Affiliated Hospital, Dalian Medical University, Dalian, Liaoning 116023; Departments of [8]Cardiovascular Medicine and [9]Hepatobiliary Surgery, The First Affiliated Hospital, Dalian Medical University, Dalian, Liaoning 116011; [10]Department of Otorhinolaryngology, The Second Affiliated Hospital, Dalian Medical University, Dalian, Liaoning 116023, P.R. China

Received January 11, 2018; Accepted June 11, 2018

DOI: 10.3892/ijo.2018.4460

Abstract. Parthenolide (PTL) is a sesquiterpene lactone compound obtained from *Tanacetum parthenium* (feverfew) and inhibits the activation of nuclear factor (NF)-κB. Epoxymicheliolide (EMCL) is a compound which is structurally related to PTL; however, EMCL is more stable under acidic and alkaline conditions. As a biologically active molecule, the detailed mechanism by which EMCL inhibits tumor activity remains to be elucidated. The present study evaluated the effect of EMCL on renal cell carcinoma (RCC) cells and identified the underlying mechanisms. It was found that treatment with EMCL significantly inhibited the proliferation of RCC cells *in vitro* and increased the induction of apoptosis by activating the mitochondria- and caspase-dependent pathway. Simultaneously, EMCL suppressed cell invasion and metastasis by inhibiting epithelial-mesenchymal transition, as observed in a microfluidic chip assay. Furthermore, using immunofluorescence analysis, an electrophoretic mobility shift assay and a dual-luciferase reporter assay, it was shown that treatment with EMCL significantly suppressed the expression of cyclooxygenase-2 by inhibiting the translocation of NF-κB p50/p65 and the activity of NF-κB. Collectively, the results indicated that EMCL suppressed tumor growth by inhibiting the activation of NF-κB and suggested that EMCL may be a novel anticancer agent in the treatment of RCC.

Correspondence to: Professor Xishuang Song, Department of Urology, The First Affiliated Hospital, Dalian Medical University, Dalian, Liaoning, 116011, P.R. China
E-mail: song-xishuang@163.com

Professor Qi Wang, Department of Respiratory Medicine, The Second Affiliated Hospital, Dalian Medical University, Dalian, Liaoning 116023, P.R. China
E-mail: wqdlmu@163.com

Key words: epoxymicheliolide, renal cell carcinoma, nuclear factor-κB, inhibitor of NF-κB kinase β, cyclooxygenase-2

Introduction

Each year, >273,000 new cases of malignant nephrotic tumors are reported worldwide, accounting for ~2% of all cases of cancer (1), among which >85% of cases are renal cell carcinomas (RCCs). RCC is considered the most life-threatening type of common urinary cancer and, despite significant progress in RCC treatment in previous years, 25-30% of patients continue to present with metastases. Patients with metastatic RCC have a poor prognosis, the median survival rate of which can be <1 year (2). Surgical resection remains the primary treatment for RCC, however, 30-40% of patients continue to present with recurrence or disease progression following surgery (3). The majority of RCC treatment failures are due to radiation not being an ideal treatment option and traditional chemotherapy not always being effective. Therefore, it is critical to identify novel therapeutic strategies and more effective agents to treat RCC, and to improve patient survival rates and quality of life.

Parthenolide (PTL) is a sesquiterpene lactone compound obtained from *Tanacetum parthenium* (feverfew). Owing to the anti-inflammatory activity of PTL, it has been used worldwide for the treatment of migraine and rheumatoid arthritis

for many years (4). Several studies have shown that PTL can inhibit the activity of nuclear factor (NF)-κB, and it has been shown in cell and animal experiments to inhibit the expression of proinflammatory cytokines (5,6). One study reported on the PTL-based treatment of RCC by inhibiting the activity of NF-κB (7). On investigating the inhibition of NF-κB activity, it was observed that PTL compounds and their derivatives are promising therapeutic agents for the treatment of different inflammatory-related diseases. It has also been reported that PTL can inhibit cell proliferation, promote apoptosis and enhance the anticancer effect of certain drugs in various types of human cancer cell *in vitro*, including non-small cell lung cancer, colon cancer, pancreatic cancer, acute myelogenous leukemia and cervical cancer (8-12). Owing to the instability of PTL in acidic and alkaline conditions (13), a structurally-related compound, epoxymicheliolide (EMCL), has been developed; however, whether EMCL can treat cancer, and its anticancer mechanism, remain to be fully elucidated.

NF-κB is an important class of transcription factor, which has a wide range of biological effects through downstream target genes, including proliferation, metastasis and apoptosis (7,14). There is increasing evidence that the NF-κB signaling pathway is the central coordinator for cancer (15). In tumors, mainly through internal or external factors, an elevated NF-κB activity is established, thereby enhancing tumor proliferation, migration and invasion (16). The NF-κB signaling pathway has been investigated in several malignancies, including RCC (17). In addition, it has been shown that RCC can be treated by inhibiting activation of the NF-κB signaling pathway (18).

The inflammatory antitumor response is important in inhibiting tumor growth in human malignancies (19). Cyclooxygenase-2 (COX-2) is a rate-limiting enzyme for the synthesis of prostaglandins from arachidonic acid, which is regulated by NF-κB (20). COX-2 regulates the formation of carcinogens, assists in tumor progression, and inhibits apoptosis, angiogenesis and the metastatic process (21). COX-2 is commonly unregulated in various types of human cancer, including RCC (22-24). *In vitro*, *in vivo*, observational and clinical data have demonstrated that selective COX-2 inhibitors are effective in preventing proliferation, angiogenesis and inflammation, and inducing apoptosis in human cancer cells (5,14,25). These findings indicate that COX-2 may be a useful target for the treatment of RCC in chemotherapeutic strategies.

In the present study, the mechanism of EMCL in inhibiting the expression of COX-2 was investigated, and it was revealed that EMCL inhibited the NF-κB/COX-2 signaling pathways by targeting leucine 21 and leucine 25 in inhibitor of NF-κB (IκB) kinase β (IKKβ) in RCC cells.

Materials and methods

Chemicals and reagents. EMCL and pyromellitic acid (PMA) were purchased from Nanjing Spring & Autumn Biological Engineering Co., Ltd. (Nanjing, China). Ammonium pyrrolidine dithiocarbamate (PDTC) and celecoxib were purchased from Sigma-Aldrich; EMD Millipore (Billerica, MA, USA). All reagents were dissolved in dimethyl sulfoxide (DMSO) as the initial concentrate and diluted with medium prior to use; the final concentration of DMSO was <0.1%. The pGL3-NF-κB plasmid, which contained four NF-κB binding motifs (GGGACTTTCC), pGL3-Basic plasmid, and pRL-TK plasmid were purchased from GenePharma (Suzhou, China). Anti-cyclin B1 (cat. no. 4138), anti-cyclin E1 (cat. no. 4129), anti-cyclin-dependent kinase 2 (CDK2) (cat. no. 2546), anti-cyclin D1 (cat. no. 2922), anti-E-cadherin (cat. no. 3195), anti-vimentin (cat. no. 12826), anti-N-cadherin (cat. no. 4061), anti-B-cell lymphoma 2 (Bcl-2) (cat. no. 15071), anti-Bcl-2-associated X protein (Bax) (cat. no. 2774), anti-cleaved caspase-3 (cat. no. 9664), anti-cleaved caspase-9 (cat. no. 7237), anti-cleaved poly (ADP-ribose) polymerase (PARP) (cat. no. 5625), anti-COX-2 (cat. no. 12282), anti-phosphorylated (p)-IKKβ (cat. no. 2697), anti-IKKβ (cat. no. 2684), anti-p-IκBα (cat. no. 2859), anti-IκBα (cat. no. 9242), anti-p65 (cat. no. 8242), anti-p-p65 (cat. no. 3033), histone H3 (cat. no. 4499) and anti-β-actin (cat. no. 3700) antibodies were purchased from Cell Signaling Technology, Inc. (Danvers, MA, USA). Anti-cytochrome *c* (cat. no. sc-13561), and anti-p50 (cat. no. sc-81710) antibodies were purchased from Santa Cruz Biotechnology, Inc. (Santa Cruz, CA, USA). Anti-matrix metalloproteinase (MMP)-2 (cat. no. ab86607), anti-MMP-9 (cat. no. ab76003) and anti-tissue inhibitor of metalloproteinase (TIMP)-2 (cat. no.ab180630) were purchased from Abcam (Cambridge, MA, USA).

Cell culture. The 786-0, Caki-1 and A498 human RCC cell lines were obtained from the American Type Culture Collection (Manassas, VA, USA). The 786-0, Caki-1 and A498 cells were cultured in RPMI-1640 medium (Gibco; Thermo Fisher Scientific, Inc., Waltham, MA, USA), McCoy's 5a modified medium (Gibco; Thermo Fisher Scientific, Inc.), and Dulbecco's modified Eagle's medium (Gibco; Thermo Fisher Scientific, Inc.), respectively, with 10% fetal bovine serum (FBS; Gibco; Thermo Fisher Scientific, Inc.), 100 U/ml penicillin and 100 ng/ml streptomycin. The cells were cultured at 37˚C in a humidified atmosphere with 5% CO_2. The authenticity of all cell lines was verified through the genomic short tandem repeat profile by Shanghai ZhongQiao Xin Zhou Biotechnology Co., Ltd. (Shanghai, China) and the cell lines were confirmed to be free of mycoplasma using a Mycoplasma Detection Kit-Quick Test (Biotool, Houston, TX, USA).

Cell Counting Kit-8 (CCK-8) assay. Cell viability was measured using a CCK-8 assay (DojindoMolecular Laboratories, Inc., Kumamoto, Japan). Briefly, $3x10^3$ cells were counted and seeded into 96-well flat-bottomed plates in 100 μl of complete medium, allowed to adhere overnight, and then treated with various concentrations of EMCL (0, 5, 10, 15, 20, 30, 50, 100 and 200 μM) for 24 and 48 h at 37˚C. CCK-8 (10 μl) was added to each well, and the absorbance was measured following incubation for 2 h at 37˚C. Each experiment was repeated at least three times.

Colony formation assay. The human RCC cells were treated with various concentrations of EMCL (0, 5, 10 and 20 μM) for 24 h, and then trypsinized to form single-cell suspensions, and seeded into 6-well plates (800 cells/well). Following incubation at 37˚C in 5% CO_2 for 14 days until colonies were

large enough to be visualized, the cells were washed with phosphate-buffered saline (PBS) and fixed in methanol/glacial acetic/ddH_2O (1:1:8) for 10 min and stained with 0.1% crystal violet for 30 min. The colonies were then photographed using a Canon camcera (PowerShot SX620 HS).

Wound-healing assay. Wound-healing assays (scratch assays) were performed to detect cell migration. Briefly, the 786-0 and Caki-1 cells were grown to full confluence in 6-well culture plates. Following 6 h of serum starvation, the confluent cell monolayer was scraped with a sterile 10-μl pipette tip and treated with the indicated doses of EMCL. After 24 h, the wound gap was observed and images were captured.

Cell invasion assay. The human RCC cells were treated with various concentrations of EMCL (0, 5, 10 and 20 μM) for 24 h. According to the manufacturer's protocol, Transwell filters were precoated with 70 μl of 1.1 mg/ml Matrigel (BD Biosciences, Franklin Lakes, NJ, USA), following inoculation of 10^5 cells per pore in 200 μl cell sap. Culture medium (600 μl) with 10% FBS was added into the lower chamber and cultured in a CO_2 incubator. After 24 h, the lower chamber cells were fixed in methanol/glacial acetic/ddH_2O (1:1:8) for 10 min and stained with 0.1% crystal violet for 30 min. Three independent experiments were performed in triplicate.

Fabrication of the microfluidic chip and in vitro cell migration/invasion assay. The microfluidic system was fabricated on a micro-patterned polydimethylsiloxane (PDMS; Sylgard 184; Dow Chemical, Midland, MI, USA) chip using the standard soft lithographic method, as described in our previous study (26). As shown in Fig. 3D, the microfluidic system consisted of a glass coverslip, a central gel micro-channel (9,000x1,000x40 μm), and two lateral media micro-channels (6,000x1,000x40 μm), which were separated by two arrays of micro-columns (200x50x40 μm). The gap between each micro-column was 50x20x40 μm. To quantify the invasive capability of the cancer cells, the gel micro-channels were precoated with Matrigel (BD Biosciences). The human RCC cells (5x10^6/ml;3 μl) pre-treated with varying concentrations of EMCL (0, 5, 10 and 20 μM) for 24 h containing 10% FBS medium were seeded into the cell micro-channel, and medium containing 20% FBS was added as a chemoattractant in the medium micro-channel. The chip was cultured in a CO_2 incubator for 24 h, following which images were captured using a Leica DM14000B microscope fitted with digital camera.

Confocal immunofluorescence analysis. The 786-0 cells were seeded on coverslips and treated with varying concentrations of EMCL (0, 5, 10 and 20 μM) for 24 h. Subsequently, the cells were fixed with 4% paraformaldehyde at room temperature, permeabilized with 0.2% Triton X-100, and blocked in PBS containing 5% bovine serum albumin (Sigma-Aldrich, St. Louis, MO, USA). The cells were washed with PBS, incubated with 3% FBS for 30 min at room temperature, and incubated overnight at 4˚C with antibodies specific to NF-κB p50 (1:100 dilution) and NF-κB p65 (1:500 dilution). Following this, the cells were incubated with fluorescein isothiocyanate- or rhodamine isothiocyanate-conjugated secondary antibodies (cat. no. 4408 or 4413, 1:1,000 dilution, Cell Signaling Technology) for 60 min at room temperature in a darkroom. Finally, DAPI was added to each sample for nuclear counterstaining, and fluorescent images were examined using a Leica DM 14000B confocal microscope (Leica Microsystems, Inc., Buffalo Grove, IL, USA).

Western blot analysis. Cell lysate preparation and western blot analysis were performed as previously described (25). Briefly, cells were lysed in lysis buffer for 30 min. The lysates were then centrifuged at 12,000 x g for 15 min at 4˚C, and the total protein concentration was determined using a BCA protein assay kit. Equivalent quantities of protein (40 μg) from each cell group were separated on a 12% SDS-PAGE gel and transferred electrophoretically onto polyvinylidene difluoride membranes (EMD Millipore). The membranes were blocked with 5% non-fat dry-milk for 1 h and then incubated overnight at 4˚C with antibodies specific to COX-2 (1:1,000 dilution), NF-κB p65 (1:1,000 dilution), IKKβ (1:1,000 dilution), IκBα (1:800 dilution), p-NF-κB p65 (1:500 dilution), p-IKKβ (1:500 dilution), p-IκBα (1:500 dilution), cyclin B1 (1:1,000 dilution), cyclin E1 (1:1,000 dilution), CDK2 (1:1,000 dilution), cyclin D1 (1:1,000 dilution), E-cadherin (1:1,000 dilution), vimentin (1:1,000 dilution), N-cadherin (1:1,000 dilution), Bcl-2 (1:1,000 dilution), Bax (1:1,000 dilution), cleaved caspase-3 (1:1,000 dilution), cleaved caspase-9 (1:1,000 dilution), cleaved caspase-PARP (1:1,000 dilution), NF-κB p50 (1:200 dilution), MMP-2 (1:500 dilution), MMP-9 (1:500 dilution), TIMP-2 (1:500 dilution), GAPDH (1:2,500 dilution), histone H3 (1:2,000 dilution) and β-actin (1:2,000 dilution). The membrane was then washed three times with 1XTris-buffered saline with Tween and incubated with the anti-rabbit IgG (1:5,000 dilution) (cat. no. 7074) or anti-mouse IgG (1:5,000 dilution) (cat. no. 7076) secondary antibodies for 2 h at room temperature. The protein bands were visualized by enhanced chemiluminescence, and the integrated optical density of bands was quantified using ImageQuant TL 7.0 (GE Healthcare Life Sciences, Chalfont, UK).

Reverse transcription-quantitative polymerase chain reaction (RT-qPCR) analysis. Total RNA was extracted from the cells using the RNAprep pure Cell kit (Tiangen Biotech Co., Ltd., Beijing, China). The cDNA was synthesized from 1 μg of total RNA as the template in a 20-μl reaction volume using the FastQuant RT kit (with gDNase; Tiangen Biotech Co., Ltd.) at 42˚C for 15 min and 95˚C for 3 min according to the manufacturer's instructions. The mRNA level of genes was detected with SuperRealPreMix Plus (SYBR-Green) from Tiangen Biotech Co., Ltd. The relative quantification for the mRNA level of the genes was performed by RT-qPCR using the Agilent Mx3005P qPCR system (Agilent Technologies, Inc., Santa Clara, CA, USA) in triplicate for each of the independently prepared RNAs. The primer sequences used were as follows: COX2 (PTGS2) forward, 5'-CAG CCA TAC AGC AAA TCC TTG-3' and reverse, 5'-CAA ATG TGA TCT GGA TGT CAA C-3'; β-actin forward, 5'-CAC CAG GGC GTG ATG GT-3' and reverse, 5'-CTC AAA CAT GAT CTG GGT CAT-3'. qPCR was performed at 95˚C for 15 min, 95˚C for 10 sec and 60˚C for 20 sec for 40 cycles. The relative levels of COX-2 transcripts were normalized to the expression of β-actin and calculated based on the $2^{-\Delta\Delta Cq}$ method (27).

Flow cytometric analysis. To determine the distribution of cells in the cell cycle and the proportion of apoptotic cells, flow cytometric analysis was performed using a flow cytometer (BD FACS Accuri C6; BD Biosciences). Briefly, the 786-0 cells were treated with different concentrations of EMCL (0, 5, 10, and 20 μM) for 24 h, following which the treated cells were collected and fixed with ice-cold 70% ethanol at 4˚C for 4 h, and then stained with propidium iodide (PI) staining buffer (0.2% Triton X-100, 100 μg/ml DNase-free RNase A, and 50 μg/ml PI in PBS) in the dark for 30 min. For apoptosis examination, the treated cells were stained with the Annexin V-FITC Apoptosis Detection kit in the dark at room temperature for 15 min. The cell cycle distribution and the fraction of apoptotic cells were determined using the FACS analysis system.

Dual-luciferase reporter assay. In the 786-0 cells, the pRL-TK plasmid was co-transfected with pGL3-NFκB or pGL3-basic (negative control) in a 96-well plate using Lipofectamine 2000 (Invitrogen; Thermo Fisher Scientific). Following treatment with different concentrations of EMCL (0, 5, 10, and 20 μM) for 24 h, the dual-luciferase reporter assay system (Promega, Madison, WI, USA) was used to measure the changes in luciferase activity. Firefly luciferase activity was normalized to *Renilla* luciferase activity. All values are shown as the mean ± standard deviation of triplicate samples.

Electrophoretic mobility shift assay (EMSA). The 786-0 cells were treated with different concentrations of EMCL (0, 5, 10, and 20 μM) for 24 h. The nuclear proteins of the human RCC cells were then isolated using the Nuclear and Cytoplasmic Protein Extraction kit (Beyotime Institute of Biotechnology, Shanghai, China) according to the manufacturer's protocol. The protein concentrations were measured using the bicinchoninic acid method. Double-stranded oligonucleotides encoding the NF-κB consensus sequence were 5'-AGT TGA GGG GAC TTT CCC AGG C-3' and 3'-TCA ACT CCC CTG AAA GGG TCC G-5', which were end-labeled with biotin (Beyotime Institute of Biotechnology). Nuclear extracts (5 μg) were added to 20 μl of binding reactions and incubated for 20 min at room temperature. The EMSA reactions were performed according to the manufacturer's protocol (Light Shift Chemiluminescent EMSA kit; Pierce; Thermo Fisher Scientific, Inc.). The same unlabeled probe was used as a competitor in the assay. Three independent experiments were performed in triplicate.

Molecular modeling. Molecular docking was used to investigate whether EMCL specifically binds to IKKβ protein complexes. EMCL was optimized using the semi-empirical PM3 method with the Polak-Ribière-Polyak conjugate gradient algorithm, with an RMS gradient of 0.01 kcal mol^{-1} $Å^{-1}$ as convergence criterion. The optimized structure of EMCL was docked into the active site of IKKβ with ligand K-252A (PDB code: 4KIK). The crystallographic ligand was extracted from the active site, and the residues within a 6.5 Å radius around the IKKβ molecule were defined as the active pocket. The Surflex-Dock of sybyl-x 1.10 program package (Tripos, St. Louis, MO, USA) was used for the docking calculations with default parameters.

Table I. Twenty-four and 48 h IC_{50} values of EMCL for inhibition of cell viability.

	IC_{50} (μM)	
Cell line	24 h	48 h
786-0	18.82±2.24	12.98±1.35
Caki 1	25.38±1.61	15.16±0.90
A498	37.58±1.58	28.95±1.46

Statistical analysis. All data are expressed as the mean ± standard deviation of at least three independent experiments. Statistical analysis was performed using SPSS 19.0 software (IBM SPSS, Armonk, NY, USA). statistical significance for each variable was estimated by a one-way analysis of variance followed by Tukey's test for post hoc analysis. $P<0.05$ was considered to indicate a statistically significant difference.

Results

EMCL inhibits RCC proliferation and changes cell morphology. In order to investigate the functional role of EMCL in human RCC cells, the present study quantitatively examined the effect of EMCL on cell morphology and cell proliferation in several human RCC cell lines. First, the effect of EMCL on cell proliferation was quantitatively examined in 786-0, Caki-1and A498 cells using a CCK-8 assay. As shown in Fig. 1A, following treatment of the three RCC cell lines with different concentrations of EMCL for 24 and 48 h, the survival rates of the three cell lines decreased in a dose- and time-dependent manner. The IC_{50} values of EMCL against the 786-0, Caki-1 and A498 cells were then calculated (Table I). As shown in Fig. 1B, EMCL reduced cell-to-cell contact and filopodia formation in the 786-0 and Caki-1 cells, compared with the cells in the DMSO vehicle control groups.

EMCL induces cell cycle arrest of RCC cell lines. As changes in cell proliferation are usually accompanied by changes in the cell cycle (28), the present study next evaluated the effect of EMCL on the cell cycle. As shown in Fig. 1C and D, induction of cell cycle arrest was observed in the G0/G1 phase. Compared with the control group, the percentages of cells in the G0/G1 phase increased from 43.2 to 67.3% and from 30.6 to 59.1% following EMCL treatment in the 786-0 and Caki-1 cells, respectively; whereas, the percentages of cells in the S phase decreased from 33.24 to 18.05% and from 29.70 to 7.67%, respectively.

Subsequently, the present study investigated the influence of EMCL on colony formation in 786-0 and Caki-1 cells by using the colony formation assay. As shown in Fig. 2A and B, treatment with EMCL resulted in a significant reduction of RCC cell colony formation and colony formation rate. These results showed that EMCL may be a potent inhibitor of RCC cell proliferation.

To determine the detailed mechanisms underlying the above, the protein expression of several core cell cycle regulators were examined by western blot analysis in human

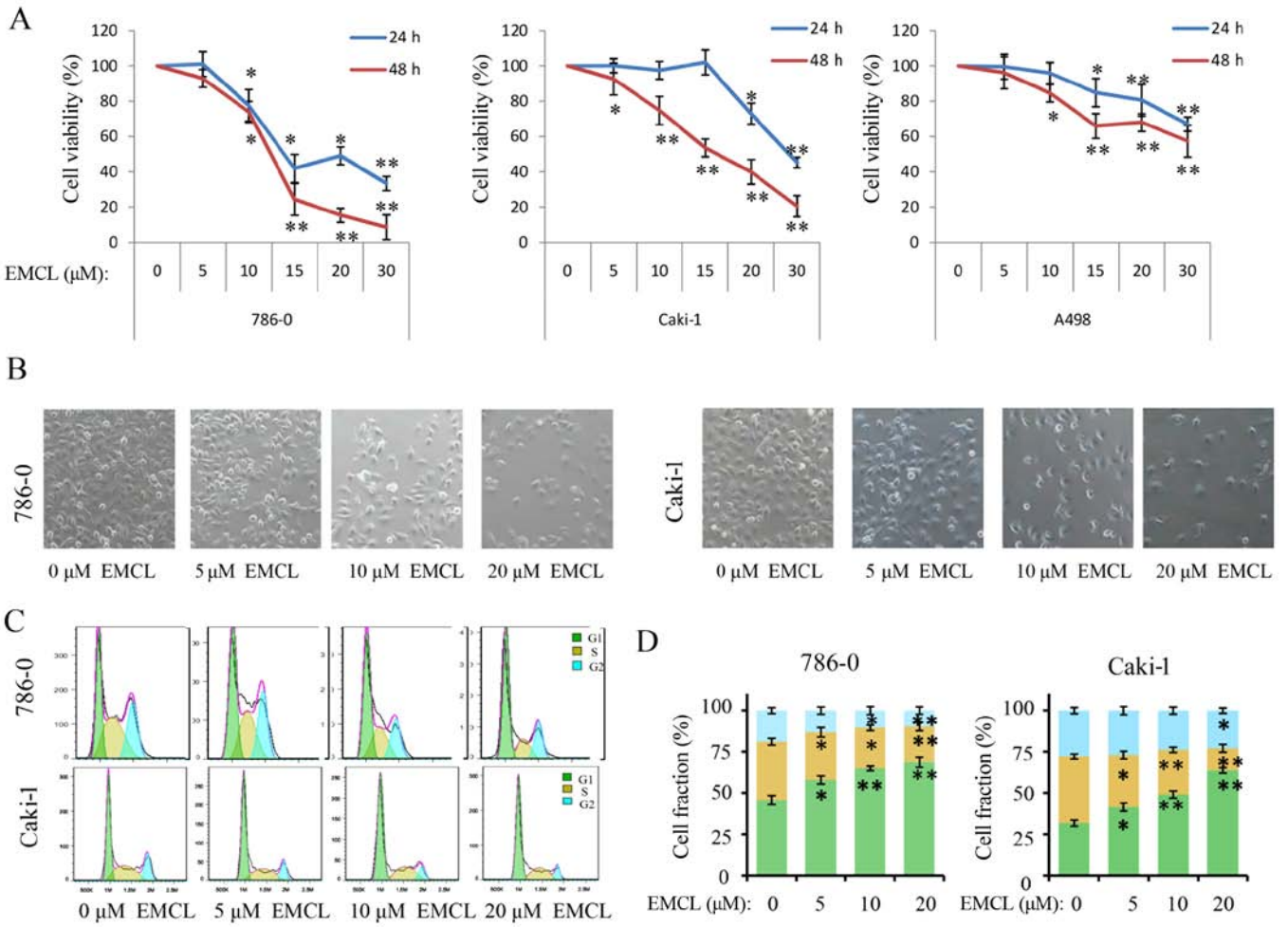

Figure 1. EMCL inhibits cell viability, changes morphology, and induces cell cycle arrest. (A) 786-0, Caki-1, and A498 cells were treated with EMCL at the indicated doses. Following treatment for 24 and 48 h, cell viability was determined using a Cell Counting Kit-8 assay. Cells treated with vehicle control (DMSO) were used as the reference group (viability set at 100%). (B) Changes in cell morphology and spreading of 786-0 and Caki-1 cells treated with EMCL at the indicated doses for 24 h were observed. Images were captured using a microscope fitted with a digital camera (magnification, x100). (C) Cell cycle analyses of 786-0 and Caki-1 cells were performed following 24 h of treatment with EMCL, using a BD Accuri C6 flow cytometer. (D) Cell fractions were calculated. Data are presented as the mean ± standard deviation of three independent experiments. *P<0.05 and **P<0.01, vs. DMSO-treated group. EMCL, epoxymicheliolide; DMSO, dimethyl sulfoxide.

RCC cells following EMCL treatment, including cyclin B1, cyclin E1, cyclin-dependent kinase 2 (CDK2) and cyclin D1 (Fig. 2C and D). It is likely that cell cycle arrest may have caused the resulting reduced expression of these proteins. These data indicated that EMCL promoted G1 cell cycle arrest and delayed entry into the S phase.

EMCL suppresses migration and invasion of RCC. To verify that EMCL inhibited cell motility, cell migration and invasion were evaluated using wound-healing and Transwell assays. As shown in Fig. 3A-C, the migratory ability of the 786-0 and Caki-1 cells was inhibited by EMCL treatment in a dose-dependent manner. The same result was obtained when the microfluidic chip was used to detect the invasive capability of cancer cells (Fig. 3D and E). These results demonstrated that EMCL inhibited cell migration and invasion. To ascertain the detailed underlying mechanisms of the effect of EMCL on cell migration and invasion, key protein markers were analyzed in the 786-0 and Caki-1 cells by western blot analysis. As shown in Fig. 3F and G, treatment with EMCL significantly upregulated the expression of E-cadherin (epithelial marker), whereas the expression of mesenchymal markers (vimentin and N-cadherin) were downregulated. Consistently, EMCL also inhibited the protein expression of MMP-2 and MMP-9 and upregulated the expression of TIMP-2 in a dose-dependent manner. These results indicated that EMCL treatment inhibited cell migration and invasion via the regulation of EMT markers and the expression of MMPs.

EMCL induces apoptosis via modulating cytochrome *c and caspase signaling*. The present study also determined whether EMCL inhibited cell proliferation associated with activation of the RCC apoptotic pathway. As shown in Fig. 4A and B, treatment with EMCL at three effective concentrations for 24 h induced 7, 10.4 and 12.2% of the 786-0 cells to become apoptotic, and 6.4, 9.2, and 15.7% of the Caki-1 cells to become apoptotic. The levels of apoptosis-related proteins, including cleaved caspase-3, cleaved caspase-9, cleaved PARP, B-cell lymphoma 2 (Bcl-2) and Bcl-2-associated X protein (Bax) were also detected in the 24 h-treated cells by western

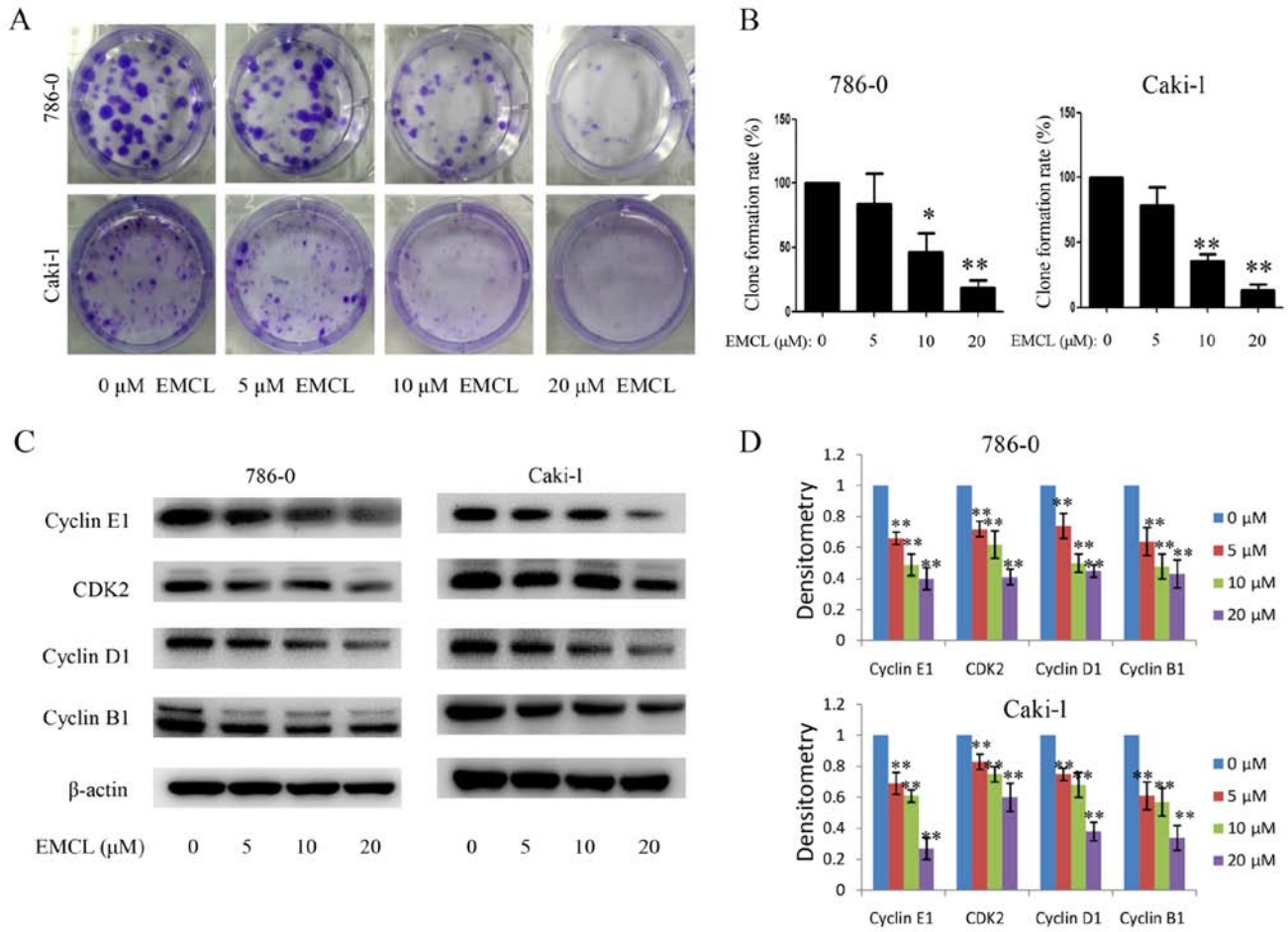

Figure 2. Effects of treatment with EMCL on cell cycle progression. 786-0 and Caki-1 cells were treated with EMCL at the indicated doses. (A) 786-0 and Caki-1 cells were treated with EMCL at the indicated doses for 24 h and images of colony formation of cells was captured. (B) Colony formation rate was calculated. (C) Protein expression levels of cyclin E1, CDK2, cyclin D1 and cyclin B1 were analyzed by western blot analysis. (D) Quantitative analysis of the proteins was performed. Data are presented as the means ± standard deviation of three independent experiments. *P<0.05 and **P<0.01, vs. dimethyl sulfoxide-treated group. EMCL, epoxymicheliolide; CDK2, cyclin-dependent kinase 2.

blot analysis. As shown in Fig. 4C-E, treatment with EMCL resulted in increased levels of cleaved caspase-3/9, cleaved PARP, and the ratio of Bax/Bcl-2.

Previous studies have shown that mitochondrial cytochrome *c* released into the cytoplasm can induce apoptosis (14,29). The present study performed immunofluorescence imaging analysis to determine whether EMCL can induce the release of cytochrome *c* in RCC cells. The results showed that treatment with EMCL effectively induced the release of cytochrome *c* from the inter-mitochondrial space into the cytosol of the 786-0 cells (Fig. 4F). These results showed that EMCL promoted the induction of cell apoptosis by triggering the release of cytochrome *c* and facilitating caspase activation in the cytosol.

EMCL suppresses the expression of COX-2 in RCC. Multiple lines of evidence and clinical data have confirmed that selective COX-2 inhibitors can suppress inflammation, angiogenesis and cell proliferation, and induce apoptosis in human cancer cells (5,16). The present study evaluated the activities of EMCL on the expression of COX-2 in human RCC cells at the protein and mRNA levels by western blot and RT-qPCR analyses, respectively. As shown in Fig. 5A and B, EMCL effectively inhibited the expression of COX-2 at the protein and mRNA levels in 786-0 cells and Caki-1 cells in a dose-dependent manner. The 786-0 and Caki-1 cells were then pretreated with the COX-2-selective inhibitor (celecoxib; CB; 50 μM) for 8 h, followed by EMCL treatment. Following incubation for 24 h, cell viability was analyzed using the CCK-8 assay. As shown in Fig. 5C, treatment with either CB or EMCL significantly inhibited cell proliferation compared with that in the controls, whereas CB pretreatment followed by EMCL treatment did not significantly alter the inhibition of cell viability, compared with EMCL treatment alone. Furthermore, the 786-0 and Caki-1 cells were incubated with EMCL following pretreatment with the COX-2 inducer PMA (200 nM) for 8 h, following which cell death was evaluated. The results showed that inducing the exogenous overexpression of COX-2 by PMA restored the cell viability of the EMCL-treated cells (Fig. 5D). These results indicated that the inhibition of proliferation by EMCL treatment of RCC cells was partially mediated by the inactivation of COX-2 signaling.

EMCL inhibits NF-κB and its binding activity. The above-mentioned results showed that EMCL inhibited the expression of COX-2; however, several transcription factors

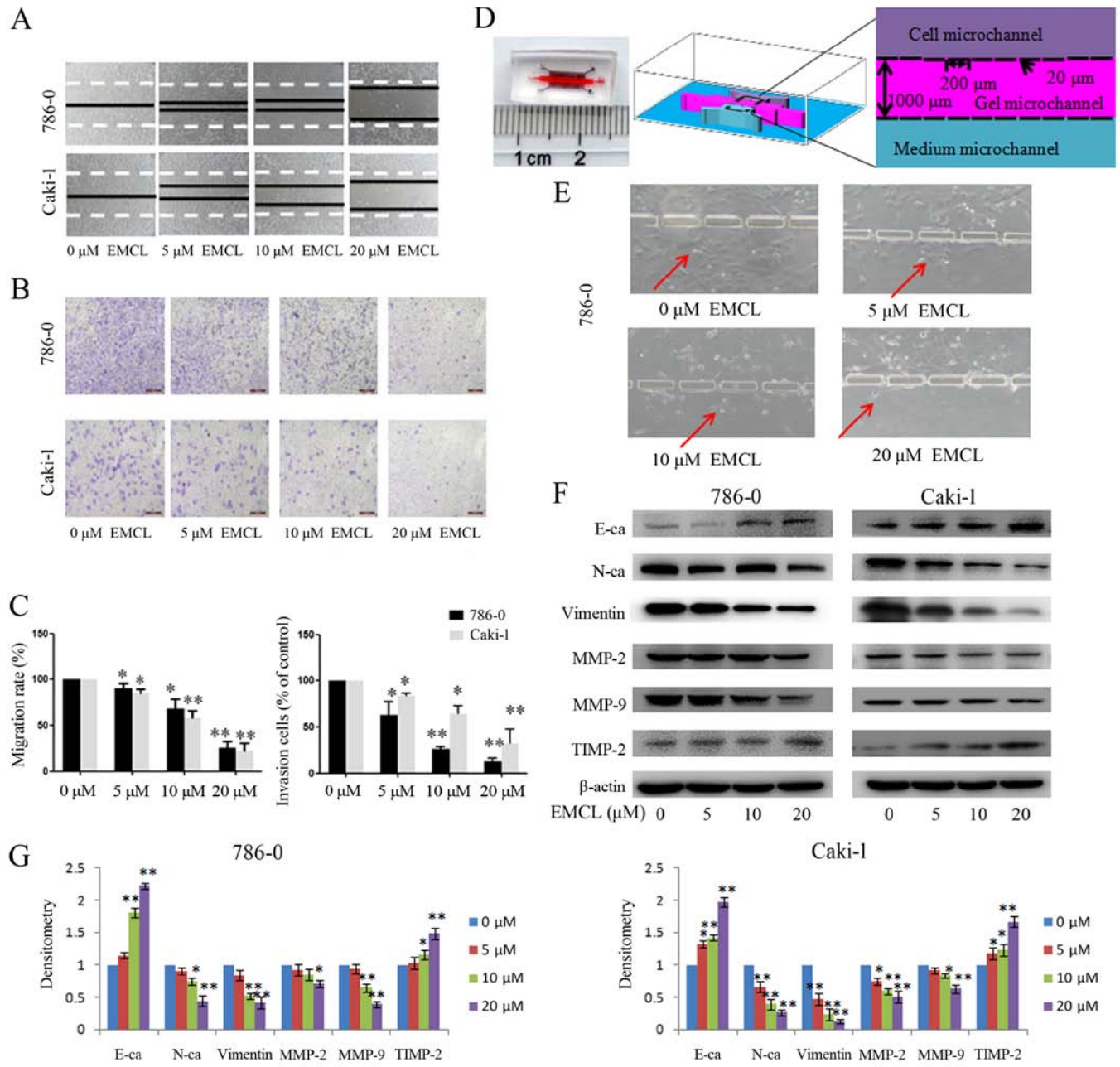

Figure 3. Effects of treatment with EMCL on cell migration and invasion. (A) Migration of 786-0 and Caki-1 cells was analyzed using a scratch assay. Following24 h of treatment with EMCL at the indicated doses, the wound gap was observed and images were captured. (B) Cell invasion was analyzed in 786-0 and Caki-1 cells treated with EMCL at the indicated doses for 24 h. Cell invasion was observed and images were captured. (C) Percentages of migrated cells were calculated relative to the original gap and the percentage of invaded cells was calculated. (D) Image and illustration of the homemade microfluidic chip. The chip comprised two-sided micro-channels sandwiching a gel micro-channel with two rows of micro-gaps. The gel micro-channel was filled with Matrigel (pink), and the cell micro-channel and medium micro-channel were used for plating the cells (purple) and the chemoattractant (20% FBS; green), respectively. (E) Invasion of 786-0 cells to the gel micro-channel following 24 h of treatment with EMCL at the indicated doses. Red arrows indicate invasion of 786-0 cells. (F) Protein expression levels of MMP-2/9, TIMP-2, E-cadherin, N-cadherin and vimentin were analyzed by western blot analysis. (G) Quantitative analysis of proteins. Data are presented as the mean ± standard deviation of three independent experiments. *P<0.05 and **P<0.01. vs. dimethyl sulfoxide-treated group. EMCL, epoxymicheliolide; E-ca, E-cadherin; N-ca, N-cadherin; MMP, matrix metalloproteinase; TIMP-2, tissue inhibitor of metalloproteinase 2.

and transcriptional coactivators affect the expression of COX-2 by regulating the promoter region of COX-2, including NF-κB (30). In the present study, the role of the NF-κB signaling pathway and their binging activity in response to EMCL challenge was examined. The EMCL concentration of 20 μM was selected as the highest treatment concentration, as it inhibited cell proliferation with only marginal cytotoxicity. In addition, selecting a concentration close to the IC_{50} can make the experimental results more obvious, therefore, in order to examine the role of NF-κB/COX-2 signaling pathway in EMCL-treated tumor cells, this concentration was selected. Firstly, the 786-0 and Caki-1 cells were pretreated with the NF-κB inhibitor PDTC (30 μM) for 6 h, followed by EMCL treatment. Following incubation for 24 h, cell viability was analyzed by the CCK-8 assay. As shown in Fig. 6A, treatment with either PDTC or EMCL significantly inhibited cell proliferation compared with that in the controls; whereas PDTC pretreatment followed by EMCL treatment did not

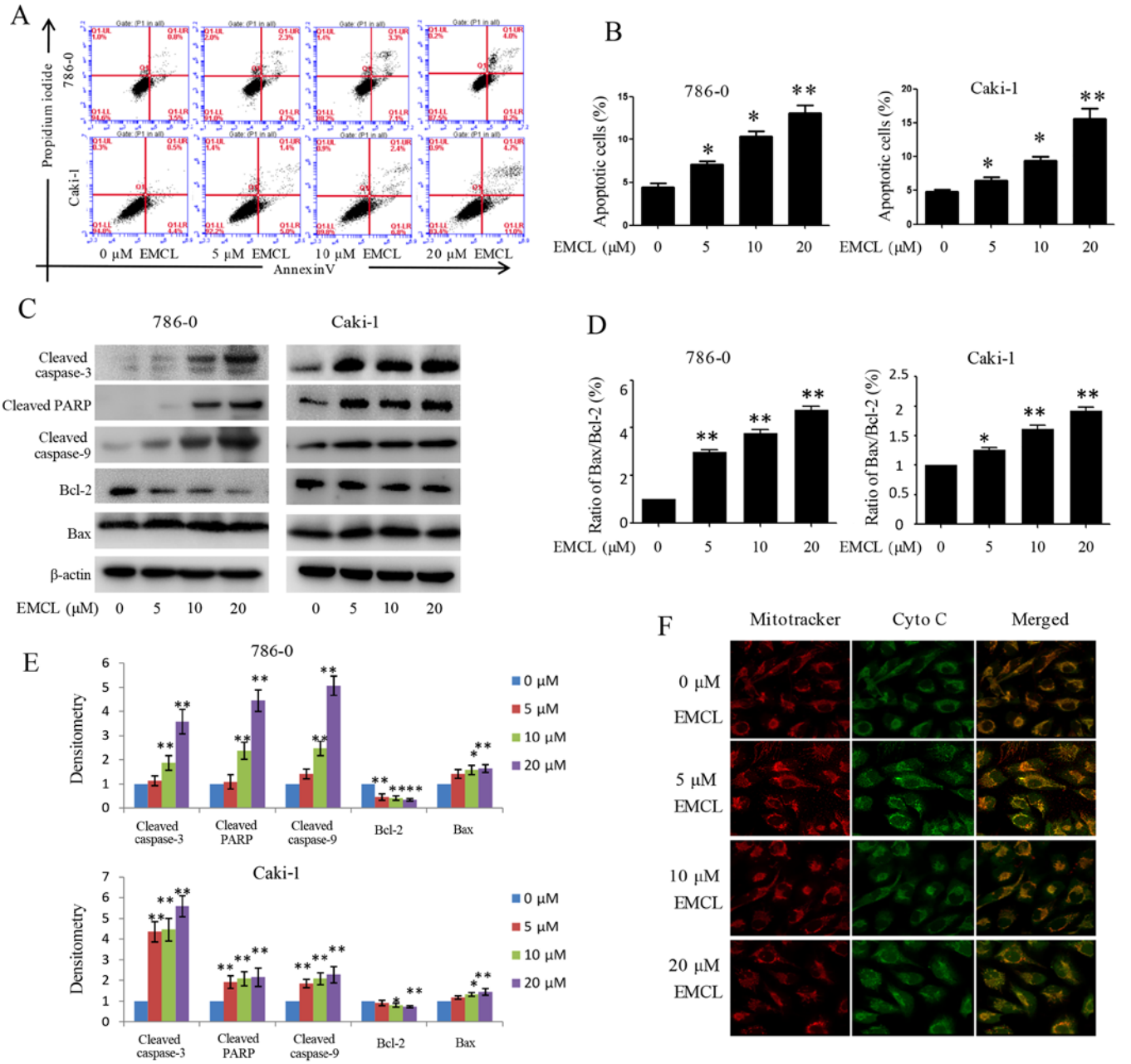

Figure 4. Effects of treatment with EMCL on caspase-dependent apoptosis. 786-0 and Caki-1 cells were treated with EMCL at the indicated doses. (A) Following treatment for 24 h, levels of apoptosis were determined by FACS analysis, (B) and the percentage of apoptotic cells was calculated. (C) Protein expression levels of cleaved caspase-3, cleaved caspase-9, cleaved caspase-PARP, and BCL-2/BAX in 786-0 and Caki-1 cells were analyzed by western blot analysis. (D) Ratio of Bax/Bcl-2. (E) Quantitative analysis of proteins. (F) Release of cytochrome *c* from the mitochondria to the cytoplasm was observed by immunofluorescence imaging analysis in 786-0 and Caki-1 cells (magnification, x630). Data are presented as the mean ± standard deviation of three independent experiments. *P<0.05 and **P<0.01, vs. dimethyl sulfoxide-treated group. EMCL, epoxymicheliolide; PARP, poly (ADP-ribose) polymerase ; Bcl-2, B-lymphoma 2; Bax, Bcl-2-assocated X protein; Cyto C, cytochrome *c*.

significantly alter the inhibition of cell viability compared with EMCL treatment alone. Furthermore, exposure of the 786-0 cells to EMCL was detected by EMSA, which indicated that EMCL treatment significantly decreased NF-κB DNA-binding activity in a dose-dependent manner (Fig. 6B). Simultaneously, the 786-0 cells were transfected with luciferase reporter plasmids containing NF-κB binding sites and treated with EMCL to investigate changes in their gene expression levels. As shown in Fig. 6C, EMCL treatment significantly suppressed gene expression by 1.2-, 1.4-, and 2.2-fold in the dual-luciferase reporter assay at the three effective concentrations of 5, 10, and 20 μM, respectively. These results indicated that inhibition of the expression of COX-2 by EMCL treatment of RCC cells was mediated by inactivation of the NF-κB signaling pathway.

EMCL inhibits NF-κB activity by targeting IKKβ. NF-κB leads to IκBα phosphorylation mainly through the activation of IKKβ kinase activity. The p-IκBα is then degraded by the proteasome, releasing the p50/p65 NF-κB dimers and activating NF-κB signaling. In the present study, the effect of EMCL on NF-κB signaling in RCC was examined. The protein changes of NF-κBp50/p65 subunits in the cytoplasm and

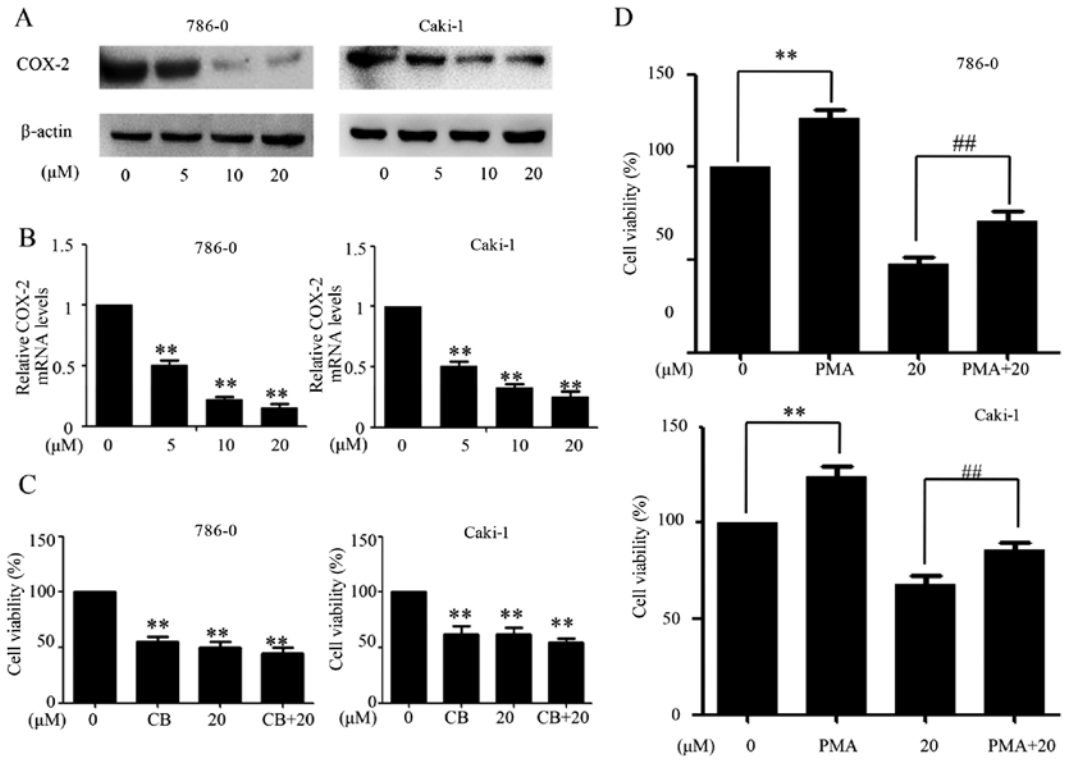

Figure 5. EMCL suppresses the expression of COX-2. 786-0 and Caki-1 cells were treated with EMCL at the indicated doses. After 24 h, expression levels of COX-2 protein and gene expression were analyzed by (A) western blot and (B) reverse transcription-quantitative polymerase chain reaction analyses in the 786-0 and Caki-1 cells, respectively. (C) 786-0 and Caki-1 cells were treated with EMCL (20 μM) for 24 h following pretreatment with the COX-2 selective inhibitor CB (50 μM) for 8 h, and the cell viability was determined by CCK-8 analysis. (D) 786-0 and Caki-1 cells were treated with EMCL (20 μM) for 24 h following pretreatment with the COX-2 selective inducer PMA (200 nM) for 8 h, and the cell viability was determined by CCK-8 analysis. Data are presented as the mean ± standard deviation of three independent experiments. **P<0.01, vs. DMSO-treated group; $^{\#\#}$P<0.01 between EMCL treatment group and combination treatment group. EMCL, epoxymicheliolide; COX-8, cyclooxygenase-2; CB, celecoxib; PMA, pyromellitic acid. CCK-8, Cell Counting Kit-8.

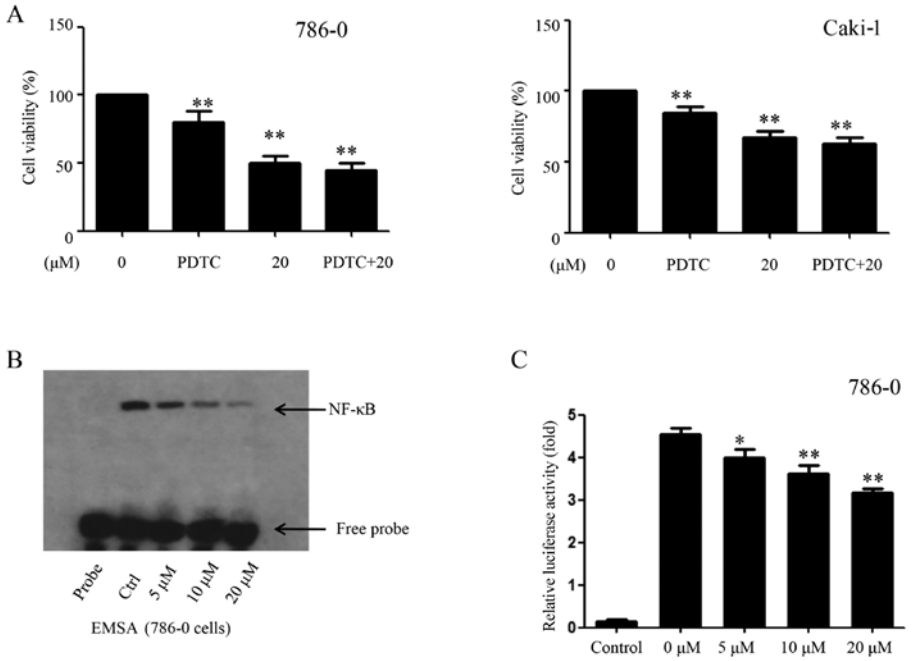

Figure 6. EMCL inhibits NF-κB and its binding activity. (A) 786-0 and Caki-1 cells were treated with EMCL (20 μM) for 24 h following pretreatment with PDTC, an inhibitor of NF-κB (30 μM), for 6 h, and the cell viability was determined by Cell Counting Kit-8 analysis. (B) 786-0 was either untreated (lane 2, control cultures) or treated with the indicated doses of EMCL (lanes 3-5) for 24 h. Nuclear extracts were prepared and analyzed by an electrophoretic mobility shift assay. (C) NF-κB-dependent gene expression in the 786-0 cell line. Cells were transfected with Bwt-luc reporter plasmid, stimulated with EMCL (5, 10, and 20 μM). These stimuli were administered 24 h following transfection, and the cell lysates were prepared following an additional 24 h incubation for the determination of luciferase activity. As an internal control, pRL-TK, expressing *Renilla* luciferase under the control of TK promoter, was co-transfected. All luciferase activities were corrected by the internal control activity of *Renilla* luciferase. Data are presented as the mean ± standard deviation of three independent experiments. *P<0.05 and **P<0.01, vs. dimethyl sulfoxide-treated group. NF-κB, nuclear factor-κB; EMCL, epoxymicheliolide; PDTC, ammonium pyrrolidine dithiocarbamate; Ctrl, control.

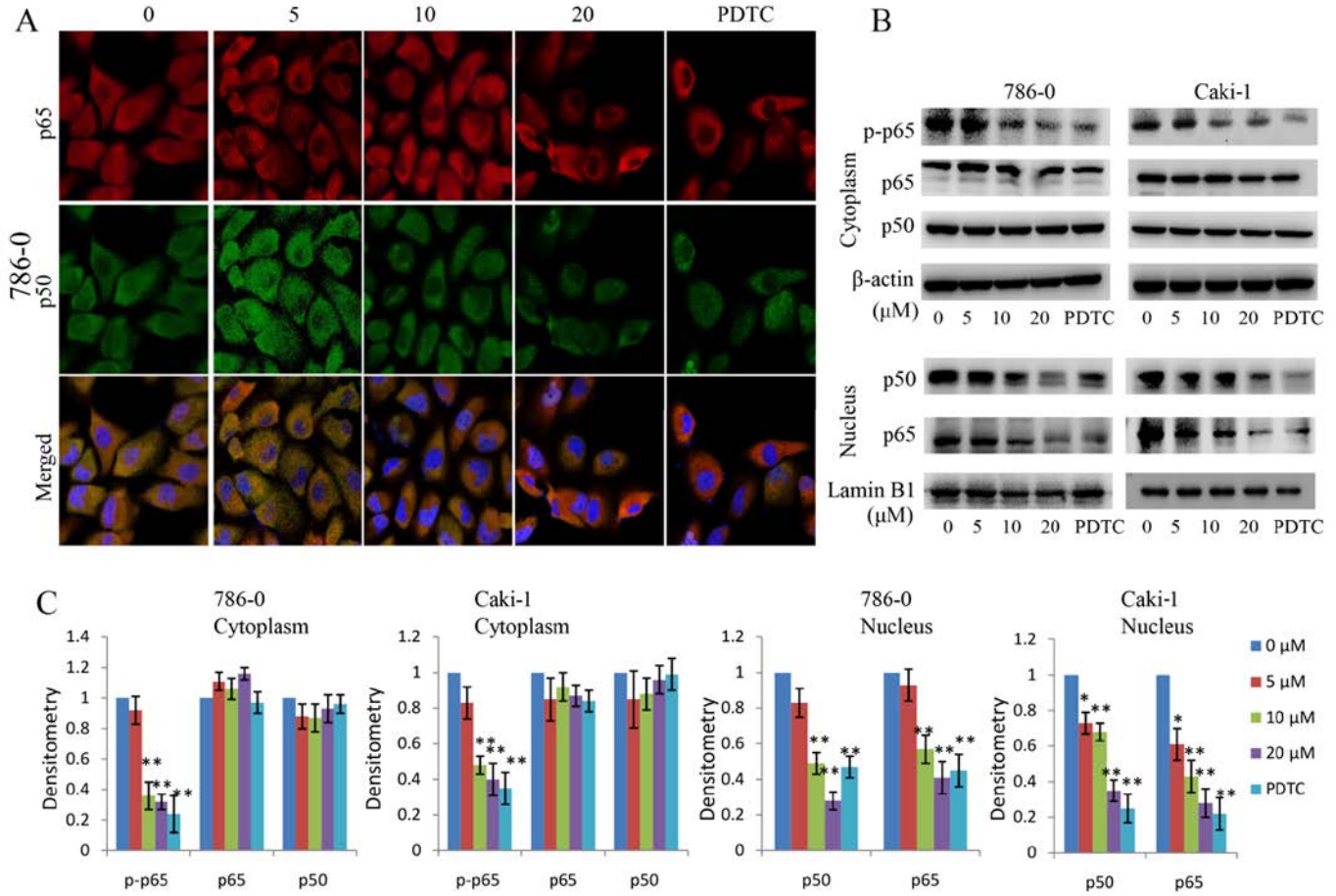

Figure 7. Effect of EMCL on nuclear factor-κB signaling. (A) Following treatment with EMCL at the indicated doses and PDTC (30 μM) for 24 h, the subcellular localizations of p50 and p65 in 786-0 cells were examined by confocal microscopy analysis(magnification, x630). (B) Following treatment with EMCL at the indicated doses and PDTC (30 μM) for 24 h, cytoplasmic and nuclear extracts were prepared for the western blot analysis of p-p65, p65, and p50. (C) Quantitative analysis of the proteins. Data are presented as the mean ± standard deviation of three independent experiments. *P<0.05 and **P<0.01, vs. dimethyl sulfoxide-treated group. EMCL, epoxymicheliolide; PDTC, ammonium pyrrolidine dithiocarbamate; p-, phosphorylated.

nuclear lysates were detected in the EMCL-treated RCC cells. As shown in Fig. 7A-C, the protein levels of p65/p50 in nuclear lysates decreased significantly following treatment with EMCL or PDTC (an inhibitor of NF-κB, used as a positive control). In addition, the protein levels of p-p65 in the cytoplasm decreased significantly following treatment with EMCL or PDTC. These data indicated that EMCL effectively inhibited activation of the NF-κB pathway in human RCC cells.

In order to determine the molecular targets of EMCL on the NF-κB pathway, the 786-0 and Caki-1 cells were treated with EMCL or PDTC, and the molecular markers of the NF-κB pathway were examined. The effects of EMCL on IκBα protein degradation and IKKβ activity were also examined. As shown in Fig. 8A and B, EMCL significantly inhibited the phosphorylation of IKKβ and IκBα, but did not affect the total IKKβ content. Subsequently, the protein levels of NF-κB p50/p65 subunits were detected in the nuclear lysates of 786-0 and Caki-1 cells treated with EMCL (20 μM) for an indicated time. The results showed that EMCL inhibited the NF-κB pathway in the 786-0 and Caki-1 cells in a time-dependent manner (Fig. 8C and D). Furthermore, the 786-0 and Caki-1 cells were treated with EMCL and NF-κB inhibitor (PDTC) alone or together, and the expression of COX-2 was detected at the mRNA and protein levels. The results showed that treatment with EMCL or PDTC alone significantly inhibited the expression of COX-2, whereas the combination of EMCL and PDTC did not significantly alter the inhibition of COX-2 at the protein or mRNA levels (Fig. 8E and F). These results indicated that the EMCL-induced inhibition of the NF-κB signaling pathway may partly involve the repression of COX-2.

Previous studies have clearly shown that the activity of IKKβ is essential for activation of the canonical NF-κB signaling pathway (14,29). From the above results, it was hypothesized that EMCL may bind to IKKβ and subsequently inhibit its kinase activity. To test this hypothesis, a computer molecular modeling assay was performed to model the interaction between EMCL and IKKβ. Molecular docking experiments predicted that EMCL was able to bind to the ATP binding site of IKKβ. As shown in Fig. 9A and B, EMCL formed two hydrogen bonds with the ATP binding pocket of the IKKβ kinase domain. The COC motif at the 9,10-epoxide moiety of EMCL formed a hydrogen bond with the backbone NH of Leu285. The OH group at the C-3 position formed an additional hydrogen bond to the carbonyl oxygen of Leu281. These computational docking results indicated that EMCL occupied the deep hydrophobic pocket in the ATP-binding site of IKKβ to inhibit its kinase activity, and then attenuated the activation of the NF-κB signaling pathway.

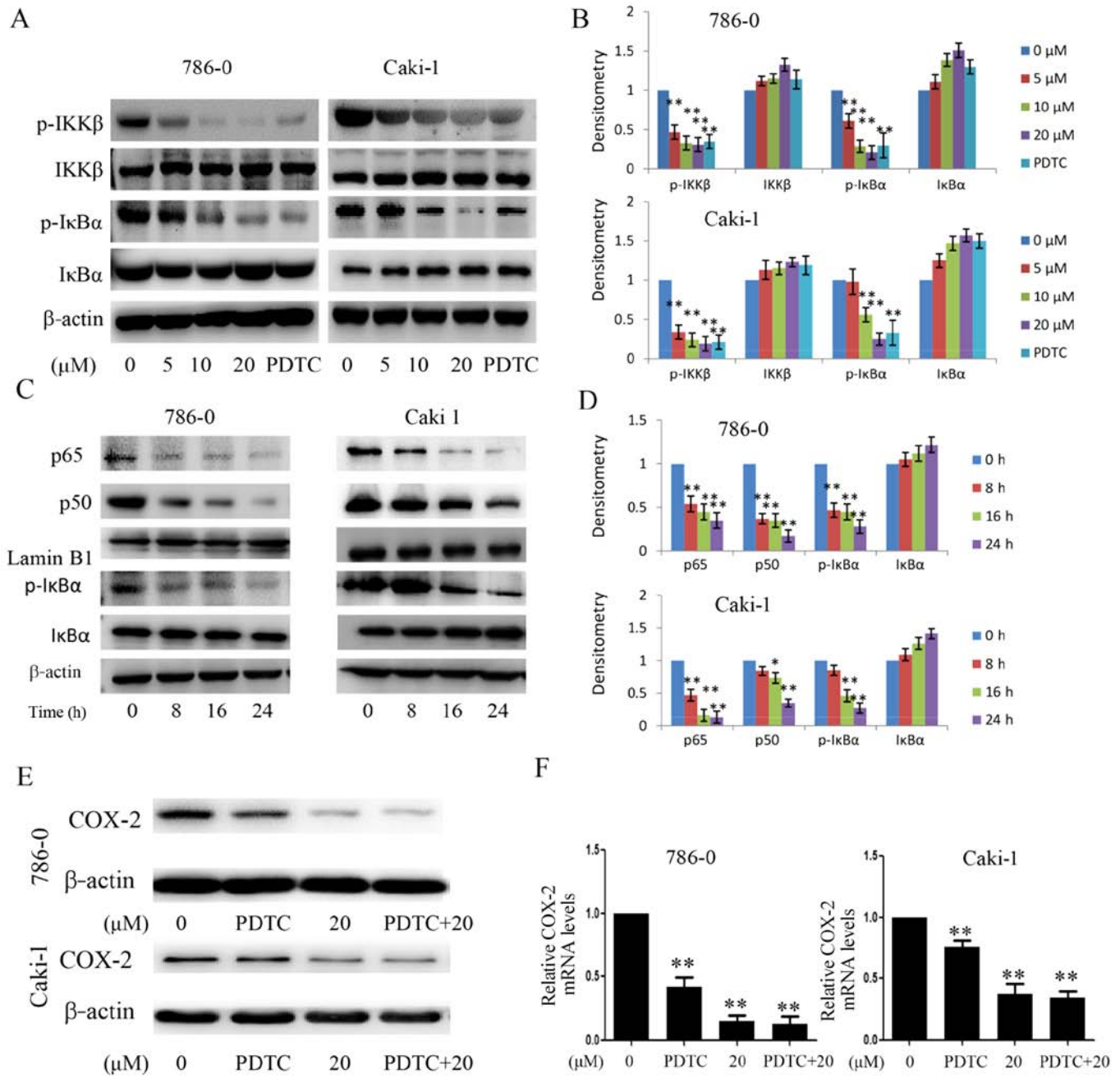

Figure 8. Effect of EMCL on IKKβ/NF-κB signaling and the expression of COX-2. (A) Following treatment with EMCL at the indicated doses and PDTC (30 μM) for 24 h, the protein expression levels of IKKβ, p-IKKβ, IκBα, and p-IκBα were analyzed by western blot analysis. (B) Quantitative analysis of the proteins. (C) Following treatment with EMCL (20 μM) at the indicated time, cytoplasmic and nuclear extracts were prepared for the western blot analysis of p65, p50, IκBα, and p-IκBα. (D) Quantitative analysis of the proteins. Following treatment with EMCL (20 μM) or PDTC (30 μM) alone or together for 24 h, protein and gene expression levels of COX-2 were analyzed by (E) western blot analysis and (F) reverse transcription-quantitative polymerase chain reaction analyses were performed in 786-0 and Caki-1 cells, respectively. Data are presented as means ± SD of three independent experiments. *P<0.05 and **P<0.01. vs. dimethyl sulfoxide-treated group. EMCL, epoxymicheliolide; PDTC, ammonium pyrrolidine dithiocarbamate; IκBα, inhibitor of nuclear factor-κB; IKK, IκB kinase; p-, phosphorylated; COX-2, cyclooxygenase-2.

All of the above results support the hypothesis that EMCL promotes the suppression of NF-κB/COX-2 signaling through the inhibition of IKKβ kinase activity.

Discussion

PTL, which is a major sesquiterpene lactone responsible for the bioactivity of feverfew, is a traditional drug that has been used for the treatment of fever, migraine, and arthritis (31). PTL exhibits significant antitumor activities, including inhibition of cell proliferation, induction of apoptosis, and enhancement of the role of anticancer drugs (8-12). As PTL is unstable under acidic and alkaline conditions (13), the structurally related compound, EMCL, was developed; however, the biological effects of EMCL *in vivo* and *in vitro* remain to be fully elucidated. In particular, to the best of our knowledge, there has been no report on the investigation of EMCL in the treatment of RCC.

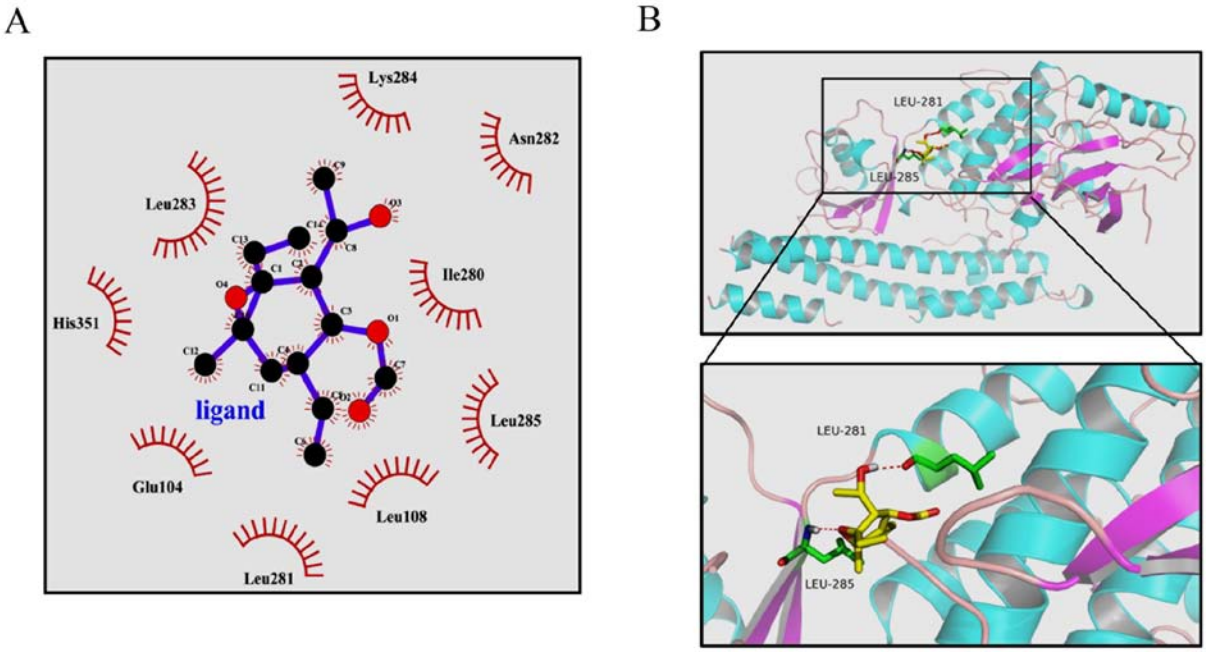

Figure 9. Highest ranked position of EMCL in the ATP-binding site of IKKβ generated with docking. (A) Interactions between EMCL and the active ATP-binding site residues of IKKβ in 2D models. (B) Interactions of EMCL and IKKβ are delineated by ribbon structure; hydrogen bonds are shown as red dashed lines, and amino acid involved residues are marked. EMCL, epoxymicheliolide; IKK, inhibitor of nuclear factor-κB kinase.

In the present study, it was found that EMCL effectively inhibited the growth of human RCC cells and enhanced the induction of apoptosis in a dose- and time-dependent manner. Furthermore, it was shown that EMCL suppressed growth and apoptosis of human RCC cells by inhibiting the NF-κB/COX-2 signaling pathway, activating the cytochrome *c*/caspase-dependent apoptotic pathway, and promoting G1 cell cycle arrest. The experiments showed that EMCL inhibited the expression of COX-2through suppressing the phosphorylation of IKKβ, preventing IκBα degradation, and resulting in the NF-κB p65/p50 protein-sustained cytoplasmic retention, thereby inhibiting its nuclear translocation and transcriptional activity. In this regard, to the best of our best knowledge, this may be the first report of the effect of EMCL on the expression of COX-2 and its potential mechanisms *in vitro*.

The inflammatory antitumor response is important in inhibiting tumor growth in human malignancies (19). COX-2, a rate-limiting enzyme for the synthesis of prostaglandins from arachidonic acid, is important in the inflammatory process. Inflammatory mediators, cytokines, growth factors and tumor promoters can rapidly induce the expression of COX-2 (30,32,33).

One of the key aspects of the inflammatory process is the association of COX-2 with the formation of carcinogens, tumor progression and inhibition of apoptosis, angiogenesis, and metastatic processes (21). COX-2 is commonly upregulated in various types of human cancer, including RCC (22-24). In order to elucidate the mechanism of EMCL as an anticancer agent, the present study investigated whether COX-2 is important in the biological activity of EMCL and found that EMCL inhibited the expression of COX-2, and inhibited the viability, migration and colony formation of human RCC cells.

The transcription factor NF-κB is key in regulating the expression of COX-2 at the transcriptional level (34). It appears likely that the mechanism by which EMCL inhibits the expression ofCOX-2 is associated with the inhibition of NF-κB in human RCC cells. In agreement with this hypothesis, the experiments in the present study showed that EMCL inhibited NF-κB signaling in human RCC cells by inhibiting phosphorylation of the IKK complex, thereby preventing IκBα degradation and resulting in sustained cytoplasmic retention of NF-κB. In the 786-0 cells, treatment with EMCL at two effective concentrations for 24 h suppressed gene expression from the reporter plasmid containing NF-κB binding sites by 1.4- and 2.2-fold, respectively. Simultaneously, exposure of the 786-0 cells to EMCL at three effective concentrations, as detected by EMSA, indicated that EMCL treatment significantly decreased NF-κB DNA-binding activity in a dose-dependent manner. Therefore, inhibition of the NF-κB pathway may be a potential mechanism involved in the suppression of human RCC cells by EMCL.

Chronic inflammation is a major activator of the metastatic cascade (35). This tumor-associated inflammation is important in regulating EMT, which contributes to cancer invasion and metastasis. The results of the present study indicated that EMCL inhibited the EMT process of RCC cells by upregulating levels of E-cadherin and downregulating levels of N-cadherin and vimentin. Activation of the MMP proteins leads to cell migration and penetration into the basement membrane, which is important in the EMT process (36). The results indicated that EMCL inhibited the protein expression and enzyme activity ofMMP-9/-2 in RCC cells. TIMPs are key endogenous regulators of MMP activity in the tissue, specifically inhibiting MMPs and maintaining matrix integrity (37). The levels of TIMP-2 were significantly increased in the EMCL-treated human RCC cells in a dose-dependent manner. These findings indicated that EMCL inhibited EMT and the synthesis of MMPs and increased TIMP-2, which is a novel finding.

In conclusion, the present study showed that EMCL is a potent suppressor of the biological characteristics of RCC with respect to cell proliferation, migration, invasion, apoptosis, and cell cycle. Furthermore, its anticancer properties were mediated, at least in part, through inhibition of the NF-κB/COX-2 signaling pathway by targeting IKKβ. These results provide evidence supporting EMCL as a novel anticancer drug for the treatment of RCC.

Acknowledgements

Not applicable.

Funding

This study was supported by the National Natural Science Foundation of China (grant nos. 81271603, 81330060 and 11472074).

Availability of data and materials

All data generated or analyzed during this study are included in this published article.

Authors' contributions

XSu, QW, and XSo conceived and designed the experiments; JiZ, JuZ, ZY, SS and CC performed the experiments; JS, WLi, WLa, JX, SL and MC conducted the statistical analysis; JiZ, JuZ, CC and MC wrote the manuscript. All authors have read and approved the final manuscript.

Ethics approval and consent to participate

Not applicable.

Patient consent for publication

Not applicable.

Competing interests

The authors declare that they have no competing interests.

References

1. Zhou S, Wang J and Zhang Z: An emerging understanding of long noncoding RNAs in kidney cancer. J Cancer Res Clin Oncol 140: 1989-1995, 2014.
2. Smaletz O: Current management and future directions in the treatment of advanced renal cell carcinoma - a latin american perspective: 10 years in review. Int Braz J Urol 41: 835-843, 2015.
3. Lu J, Wei JH, Feng ZH, Chen ZH, Wang YQ, Huang Y, Fang Y, Liang YP, Cen JJ, Pan YH, *et al*: miR-106b-5p promotes renal cell carcinoma aggressiveness and stem-cell-like phenotype by activating Wnt/β-catenin signalling. Oncotarget 8: 21461-21471, 2017.
4. Heinrich M, Robles M, West JE, Ortiz de Montellano BR and Rodriguez E: Ethnopharmacology of Mexican asteraceae (Compositae). Annu Rev Pharmacol Toxicol 38: 539-565, 1998.
5. Liao K, Xia B, Zhuang QY, Hou MJ, Zhang YJ, Luo B, Qiu Y, Gao YF, Li XJ, Chen HF, *et al*: Parthenolide inhibits cancer stem-like side population of nasopharyngeal carcinoma cells via suppression of the NF-κB/COX-2 pathway. Theranostics 5: 302-321, 2015.
6. Saadane A, Masters S, DiDonato J, Li J and Berger M: Parthenolide inhibits IkappaB kinase, NF-kappaB activation, and inflammatory response in cystic fibrosis cells and mice. Am J Respir Cell Mol Biol 36: 728-736, 2007.
7. Oka D, Nishimura K, Shiba M, Nakai Y, Arai Y, Nakayama M, Takayama H, Inoue H, Okuyama A and Nonomura N: Sesquiterpene lactone parthenolide suppresses tumor growth in a xenograft model of renal cell carcinoma by inhibiting the activation of NF-kappaB. Int J Cancer 120: 2576-2581, 2007.
8. Lin M, Bi H, Yan Y, Huang W, Zhang G, Zhang G, Tang S, Liu Y, Zhang L, Ma J, *et al*: Parthenolide suppresses non-small cell lung cancer GLC-82 cells growth via B-Raf/MAPK/Erk pathway. Oncotarget 8: 23436-23447, 2017.
9. Kim SL, Kim SH, Park YR, Liu YC, Kim EM, Jeong HJ, Kim YN, Seo SY, Kim IH, Lee SO, *et al*: Combined parthenolide and balsalazide have enhanced antitumor efficacy through blockade of NF-κB activation. Mol Cancer Res 15: 141-151, 2017.
10. Liu W, Wang X, Sun J, Yang Y, Li W and Song J: Parthenolide suppresses pancreatic cell growth by autophagy-mediated apoptosis. OncoTargets Ther 10: 453-461, 2017.
11. Pei S, Minhajuddin M, D'Alessandro A, Nemkov T, Stevens BM, Adane B, Khan N, Hagen FK, Yadav VK, De S, *et al*: Rational design of a parthenolide-based drug regimen that selectively eradicates acute myelogenous leukemia stem cells. J Biol Chem 291: 21984-22000, 2016.
12. Jeyamohan S, Moorthy RK, Kannan MK and Arockiam AJ: Parthenolide induces apoptosis and autophagy through the suppression of PI3K/Akt signaling pathway in cervical cancer. Biotechnol Lett 38: 1251-1260, 2016.
13. Jin P, Madieh S and Augsburger LL: The solution and solid state stability and excipient compatibility of parthenolide in feverfew. AAPS PharmSciTech 8: E105, 2007.
14. Yu Z, Guo W, Ma X, Zhang B, Dong P, Huang L, Wang X, Wang C, Huo X, Yu W, *et al*: Gamabufotalin, a bufadienolide compound from toad venom, suppresses COX-2 expression through targeting IKKβ/NF-κB signaling pathway in lung cancer cells. Mol Cancer 13: 203, 2014.
15. Karin M: Nuclear factor-kappaB in cancer development and progression. Nature 441: 431-436, 2006.
16. Mantovani A, Allavena P, Sica A and Balkwill F: Cancer-related inflammation. Nature 454: 436-444, 2008.
17. Kankaya D, Kiremitci S, Tulunay O and Baltaci S: Gelsolin, NF-κB, and p53 expression in clear cell renal cell carcinoma: Impact on outcome. Pathol Res Pract 211: 505-512, 2015.
18. Peri S, Devarajan K, Yang DH, Knudson AG and Balachandran S: Meta-analysis identifies NF-κB as a therapeutic target in renal cancer. PLoS One 8: e76746, 2013.
19. Ohshima H, Tazawa H, Sylla BS and Sawa T: Prevention of human cancer by modulation of chronic inflammatory processes. Mutat Res 591: 110-122, 2005.
20. Surh YJ, Chun KS, Cha HH, Han SS, Keum YS, Park KK and Lee SS: Molecular mechanisms underlying chemopreventive activities of anti-inflammatory phytochemicals: Down-regulation of COX-2 and iNOS through suppression of NF-kappa B activation. Mutat Res 480-481: 243-268, 2001.
21. Dannenberg AJ, Altorki NK, Boyle JO, Dang C, Howe LR, Weksler BB and Subbaramaiah K: Cyclo-oxygenase 2: A pharmacological target for the prevention of cancer. Lancet Oncol 2: 544-551, 2001.
22. Williams CS, Mann M and DuBois RN: The role of cyclooxygenases in inflammation, cancer, and development. Oncogene 18: 7908-7916, 1999.
23. Erdem H, Aydin HR, Bahadir A, Gündogdu B, Balta H, Sener E, Kayikci MA, Albayrak A and Erdogan F: Relationship of CD95 and COX-2 in renal cell carcinomas with survival and other prognostic parameters: A tissue microarray study. J Pak Med Assoc 65: 597-601, 2015.
24. Yang S, Gao Q and Jiang W: Relationship between tumour angiogenesis and expression of cyclo-oxygenase-2 and vascular endothelial growth factor-A in human renal cell carcinoma. J Int Med Res 43: 110-117, 2015.
25. Shrestha S, Zhu J, Wang Q, Du X, Liu F, Jiang J, Song J, Xing J, Sun D, Hou Q, *et al*: Melatonin potentiates the antitumor effect of curcumin by inhibiting IKKβ/NF-κB/COX-2 signaling pathway. Int J Oncol 51: 1249-1260, 2017.
26. Zhao H, Wang J, Kong X, Li E, Liu Y, Du X, Kang Z, Tang Y, Kuang Y, Yang Z, *et al*: CD47 promotes tumor invasion and metastasis in non-small cell lung cancer. Sci Rep 6: 29719, 2016.

27. Livak KJ and Schmittgen TD: Analysis of relative gene expression data using real-time quantitative PCR and the 2(-Delta Delta C(T)) Method. Methods 25: 402-408, 2001.
28. Hu Q, Hou YC, Huang J, Fang JY and Xiong H: Itraconazole induces apoptosis and cell cycle arrest via inhibiting Hedgehog signaling in gastric cancer cells. J Exp Clin Cancer Res 36: 50, 2017.
29. Wang X, Yu Z, Wang C, Cheng W, Tian X, Huo X, Wang Y, Sun C, Feng L, Xing J, *et al*: Alantolactone, a natural sesquiterpene lactone, has potent antitumor activity against glioblastoma by targeting IKKβ kinase activity and interrupting NF-κB/COX-2-mediated signaling cascades. J Exp Clin Cancer Res 36: 93, 2017.
30. Zhang C, Su ZY, Wang L, Shu L, Yang Y, Guo Y, Pung D, Bountra C and Kong AN: Epigenetic blockade of neoplastic transformation by bromodomain and extra-terminal (BET) domain protein inhibitor JQ-1. Biochem Pharmacol 117: 35-45, 2016.
31. Knight DW: Feverfew: Chemistry and biological activity. Nat Prod Rep 12: 271-276, 1995.
32. Boolbol SK, Dannenberg AJ, Chadburn A, Martucci C, Guo XJ, Ramonetti JT, Abreu-Goris M, Newmark HL, Lipkin ML, DeCosse JJ, *et al*: Cyclooxygenase-2 overexpression and tumor formation are blocked by sulindac in a murine model of familial adenomatous polyposis. Cancer Res 56: 2556-2560, 1996.
33. Zimmermann KC, Sarbia M, Weber AA, Borchard F, Gabbert HE and Schrör K: Cyclooxygenase-2 expression in human esophageal carcinoma. Cancer Res 59: 198-204, 1999.
34. Heiss E, Herhaus C, Klimo K, Bartsch H and Gerhäuser C: Nuclear factor kappa B is a molecular target for sulforaphane-mediated anti-inflammatory mechanisms. J Biol Chem 276: 32008-32015, 2001.
35. Lee DF and Hung MC: Advances in targeting IKK and IKK-related kinases for cancer therapy. Clin Cancer Res 14: 5656-5662, 2008.
36. Horejs CM: Basement membrane fragments in the context of the epithelial-to-mesenchymal transition. Eur J Cell Biol 95: 427-440, 2016.
37. Gomez DE, Alonso DF, Yoshiji H and Thorgeirsson UP: Tissue inhibitors of metalloproteinases: Structure, regulation and biological functions. Eur J Cell Biol 74: 111-122, 1997.